A Two-Stage Power Allocation-Based NOMA Architecture for Optical Camera Communication

Md. Shahjalal, *Student Member, IEEE*, Moh. Khalid Hasan, *Member, IEEE*, Md. Mainul Islam, *Graduate Student Member, IEEE*, Mostafa Zaman Chowdhury, *Senior Member, IEEE*, and Yeong Min Jang, *Member, IEEE*

***Abstract*—Visible light communication (VLC) is an emerging technology that provides ubiquitous connectivity by complementing radio frequency communication for the fifth-generation (5G) wireless communication and beyond. However, inadequacies in modulation bandwidth of light-emitting diode (LED) reduce the achievable data rate for image sensor-based VLC, also known as optical camera communication (OCC). Hence, for densely deployed OCC networks, multiple channel access is a major challenge faced when supporting large numbers of users. This article proposes an optical nonorthogonal multiple access based OCC (NOMA-OCC) system, where each LED can transmit two separate signals of two different power levels by superimposing them into one signal. An image sensor based receiver system is designed to separate these two signals supporting two users by implying an intensity threshold. The distinct channel capacities for both the users as well as the sum rate of the LED access point were analyzed. In order to validate the proposed NOMA-OCC scheme, the bit error rate performance of the system is also investigated through simulation for both channels and then compared with the conventional frequency shift ON–OFF keying scheme.**

***Index Terms*—Image sensor (IS), light-emitting diode (LED), nonorthogonal multiple access (NOMA), optical camera communication (OCC), visible light communication (VLC).**

I. Introduction

OPTICAL wireless communication is considered a robust candidate for the fifth-generation (5G) and beyond 5G (B5G) communications, as it paves the way for the utilization of wide optical terahertz bands for future communication [1]–[3]. Moreover, B5G communication requires massive user connectivity and heterogeneous backhaul network support. Along with many other emerging technologies, optical wireless communication (OWC) systems, such as free-space optical, light fidelity, visible light communication (VLC), and optical camera communication (OCC), have also attracted great attention in both academia and industry for supporting next-generation wireless communication systems. VLC systems use mainly two types of receivers to receive information from visible light sources [i.e., light-emitting diodes (LEDs)]. Those are p-i-n based receivers and avalanche photodiode (APD) based receivers. Both of them have a fast response and higher sensitivity; however, the cost of APD-based receiver is comparatively high. An image sensor (IS) is another type of receiver that can also receive information from visible LEDs as well as infrared LEDs, which is commonly termed as OCC [4]–[6]. Although the OCC receiver has slow response and lower sensitivity, it can receive data from multiple sources simultaneously by providing comparatively longer communication distance [7], [8]. Recently, several research articles have been published on different smart Internet of Things applications based on OCC system, such as indoor mobile robot localization [9]–[12], smart lighting, augmented reality [13], autonomous vehicular communication [14], [15], indoor patient monitoring [16], and transportation [16]–[19]. However, availability of high rate OCC is a major concern arisen due to the limitation of current camera frame rates (FR) [20] and narrow modulation bandwidth of the light source [21]. Current research shows very low data rates (up to several bits per second) for OCC at a distance of a few meters using conventional modulation schemes [22], [23].

To increase the capacity of such networks, nonorthogonal multiple access (NOMA) modulation technique can be implemented as a promising candidate. Power domain NOMA allows sharing the same time and frequency slots with different users by changing the transmission power [24], [25]. The transmitter sends the signals of different power levels by applying superposition coding [21]. More power is allocated to users of lower channel gain and vice versa. To apply this NOMA technique for VLC, the LED is set to flicker at different power levels in accordance with the signals. In order to avoid the issue of visual flickering, the transmitted signals are modulated at a higher frequency that is not visible to human eye. In recent times, NOMA has been proposed for several VLC-based network architectures to improve user throughput and reduce bit-error-rate (BER) [21], [25]–[29].

Manuscript received April 6, 2020; revised June 15, 2020, July 21, 2020, and August 5, 2020; accepted August 6, 2020. Date of publication August 27, 2020; date of current version August 26, 2021. This research was supported in part by the Ministry of Science and ICT, (MSIT) Korea, under the Information Technology Research Center (ITRC) support program (IITP-2018-0- 01396) supervised by the Institute for Information & communications Technology Promotion (IITP); in part by the Institute for Information and Communications Technology Promotion (IITP) Grant through the Korea Government (MSIT) under Grant 2017-0-00824, and the Development of Intelligent and Hybrid OCC-LiFi Systems for Next Generation Optical Wireless Communications. *(Corresponding author: Yeong Min Jang.)*

Md. Shahjalal, Moh. Khalid Hasan, Md. Mainul Islam, and Yeong Min Jang are with the Department of Electronics Engineering, Kookmin University, Seoul 02707, South Korea (e-mail: mdshahjalal26@ieee.org; khalidrahman45@ieee.org; mainul.islam@ieee.org; yjang@kookmin.ac.kr).

Mostafa Zaman Chowdhury is with the Department of Electrical and Electronic Engineering, Khulna University of Engineering and Technology, Khulna 9203, Bangladesh (e-mail: mzceee@ieee.org).

Digital Object Identifier 10.1109/JSYST.2020.3015766

Optical NOMA (O-NOMA) in VLC networks was proposed in [27]. This approach can utilize the entire available frequency band and improve spectral efficiency. NOMA was classified into two major parts for VLC, such as the power domain NOMA and the code domain NOMA. The authors utilized O-NOMA with successive interference cancellation between two receivers with different power values assigned to each receiver by applying superposition coding. It was examined through simulation that their approach achieved a data rate that was two times greater than that of a conventional orthogonal frequency-division multiple access system with a considerably reduced BER. An additional study on NOMA for VLC was proposed in [21]. An indoor scenario with multiple LEDs was considered in which the LED field-of-illumination (FOI) could be slightly overlapped. This involved the LEDs transmitting multiple signals of separate power levels using the NOMA approach. In this case, the user at the cell boundary would experience the signals of different power levels. NOMA for downlink VLC was proposed in [28]. In this scheme, two users accessed information from a single LED while ensuring outperforming throughputs and BER reduction compared with conventional orthogonal multiple access (OMA) techniques. Optimal power allocation strategies for VLC NOMA were introduced considering two theorems: the sum-rate maximization and the max–min fairness power allocation. The authors achieved a larger sum rate of the NOMA VLC system compared with the OMA scheme. There are several research works on the NOMA-based VLC systems where the receivers are typically photodiodes, whereas OCC systems use ISs as a receiver and exhibits several challenges of increasing its data rate using the conventional modulation schemes. Hence, we designed such an OCC system based on NOMA technique. The main advantage of NOMA over other techniques is the opportunity transmitting signal in power domain simultaneously. As the OCC systems are considered for short-range and line-of-sight (LOS) communications, the power variation at very high speed can provide an efficient multiple access simultaneously within several users by providing an increased sum rate.

In this article, a novel two-stage power domain NOMA-OCC system supporting two users per single LED access point (AP) is designed. This system allows both users to access two nonorthogonal (i.e., superimposed) channels of the same frequency. Individual channel signals are modulated by the method of frequency shift ON–OFF keying (FSOOK) using frequencies beyond the level of visual flickering. This article seeks to achieve two goals: first, to suggest a novel power domain NOMA for increasing OCC throughputs for the first time and second, to develop a complete transmitter and IS-based receiver system in an indoor multi-LED downlink network where each LED can provide access to two users. The individual channel capacity for both users as well as the sum rate of the LED AP are investigated to analyze the performance of the proposed scheme. After which for each user, the maximum available throughputs at different distances are compared at different camera FR (low, medium, and high). The comparison indicates that 1, 8, and 32 kb/s data rate can be achieved using 30, 240, and 960 ft/s cameras, respectively. In addition, the BER performance is compared with the conventional FSOOK system. It shows that the proposed NOMA-OCC scheme demonstrated better performance for both receivers.

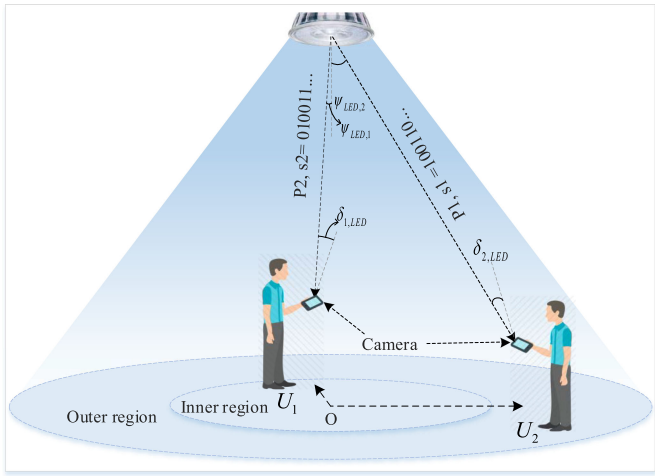

Fig. 1. Scenario of proposed NOMA scheme for OCC.

The rest of this article is organized as follows. Section II describes the system model for the proposed NOMA-OCC channel architecture in an indoor scenario. Section III presents the encoding and superimposing technique and the proposed algorithm of the LED signals in the transmitter. The IS-based receiver for receiving the signals of different power is designed on the basis of the intensity threshold in Section IV. The necessary simulation results, such as sum rate, channel capacity, and the BER analysis, are presented in Section V. Finally, the article is summarized in Section VI.

II. System Model

A. System Architecture

In a conventional OCC system, data are transmitted by modulating the light at its full and zero voltage levels. Unlike this approach, this article proposes a two-level power transmission through an LED transmitter to support NOMA in the OCC system (NOMA-OCC). Consider an LED that transmits two separate digital data s_1 and s_2 by superimposition, as illustrated in Fig. 1. The data s_1 and s_2 are transmitted through a higher power level P_1 and a lower power level P_2, respectively. In this case, flickering of the LED light within its varied power level is not an issue because the undersampled FSOOK was used at a frequency level between 2–4 kHz, whereas, the human eye can perceive visual flickering up to 200 Hz [30]. The modulation frequency for both signals remains the same and does not affect one another. The details of the NOMA-OCC superposition concept are discussed in the following sections. Assuming user 1, U_1 and user 2, U_2 want to receive information from the same LED at the same time using a smartphone camera, where U_1 is located at a distance closer to the LED than U_2. As a result, U_1 will experience higher channel gain than U_2 and receive the data s_2, which conveys a lower power level of the LED. Alternatively, U_2 will receive the information from s_1 containing a higher power level. In this case, a smartphone application should utilize the

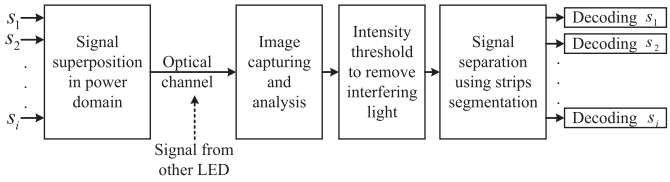

Fig. 2. Illustration of NOMA-OCC principle.

channel selection algorithm by applying an intensity threshold between the received data streams.

B. Channel Modeling

The NOMA-OCC principle is illustrated in Fig. 2. According to the principle of NOMA, bipolar signals for different users are superimposed in the power domain. In this NOMA-OCC system, these superimposed signal is sent through an optical channel at a very high carrier frequency beyond the perceivable range of the human eye. As OCC systems use IS as a receiver, it initially receives LED ON–OFF strips image of various intensity levels. Thus to receive the desired signal, successive interference cancellation is performed by intensity threshold over the received strips.

The channel estimation equations can be derived for the system as follows. The total transmitted signal can be represented as

$$T_{\text{LED}} = \frac{1}{2}\sum_{i\epsilon N}(P_{\text{high}}s_{i,\text{high}} + P_{\text{low}}s_{i,\text{low}}) \tag{1}$$

where P_{high} and P_{low} are the high and low power level of the LED, respectively. $s_{i,\text{high}}$ and $s_{i,\text{low}}$ are the two signals modulated at each power level, respectively. The received signal at the receiver can be written as

$$Y_r = (1-\alpha)a_{\text{RoI}}\xi H_{\text{LED},r}T_{\text{LED}} + \eta \tag{2}$$

where $H_{\text{LED},r}$ represents the dc channel gain to the receiver from the target LED, ξ denotes the optical to electrical conversion efficiency per pixel, a_{RoI} is the area of projected image in the IS, α is defined as the image distortion factor, and η represents the white Gaussian noise matrix with zero mean. η can be expressed as $\eta \sim NC(0,\sigma^2,I_N)$, where σ^2 is the noise variance. Visible light channel response can be represented as

$$H_{\text{LED},r} = \begin{cases} (\frac{g_r}{D^2_{r,\text{LED}}})L_m\cos(\delta_{r,\text{LED}}) \\ o \end{cases}$$
$$0 \le \delta_{r,\text{LED}} \le \theta_{\text{FOI}}$$
$$\delta_{r,\text{LED}} > \theta_{\text{FOI}} \tag{3}$$

where g_r represents optical concentrator gain of the IS, $L_m = ((m+1)/2\pi)\cos^m(\psi_{\text{LED},r})$ represents the Lambertian radiant intensity of the transmitter with order m, $\delta_{r,\text{LED}}$ represents the angle of incidence with respect to camera axis, $\psi_{\text{LED},r}$ denotes the angle of irradiance with respect to LED axis, and θ_{FOI} represents LED FOI. $D_{r,\text{LED}}$ is the direct distance between LED and the receiver camera. As camera IS comprises n number of pixels, then we can represent g_r as

$$g_r = \begin{cases} \frac{(\gamma^2 n\nu^2)}{\sin(\delta_r,\text{LED})}, & 0 \le \delta_{r,\text{LED}} \le \theta_{\text{FOI}} \\ 0, & \delta_{r,\text{LED}} > \theta_{\text{FOI}} \end{cases} \tag{4}$$

where ν is the unit pixel dimension of the IS and γ represents the receiver's refractive index. Finally, we can express the OCC channel gain as

$$H_{\text{LED},r} = \begin{cases} (\frac{(m+1)\gamma^2 n\nu^2}{2\pi D^2_{r,\text{LED}}})\cos^m(\psi_{\text{LED},r})\cot(\delta_{r,\text{LED}}) \\ 0 \end{cases}$$
$$0 \le \delta_{r,\text{LED}} \le \theta_{\text{FOI}}$$
$$\delta_{r,\text{LED}} > \theta_{\text{FOI}}. \tag{5}$$

Lower distance between the LED and camera provides higher channel gain and this helps to determine easily the power level that should be used by the receivers. We carry out the analytics of density functions of the channel gain within the LED cell region. From Fig. 1, we can represent $D_{r,\text{LED}} = \sqrt{h^2+x_r^2}$, $\cos(\psi_{\text{LED},r}) = h/\sqrt{h^2+x_r^2}$, and $\cot(\delta_{r,\text{LED}}) = h/x_r$, where h and x_r represent the vertical and horizontal distance from receiver to LED, respectively. Substituting those values in (5), the channel gain within $0 \le \delta_{r,\text{LED}} \le \theta_{\text{FOI}}$ can be represented as

$$H_{\text{LED},r} = \frac{(m+1)\gamma^2 n\nu^2}{2\pi\sqrt{h^2+x_r^2}}.\frac{h^m}{(h^2+x_r^2)^{m/2}}.\frac{h}{x_r}$$
$$= \frac{K(m+1)h^{m+1}}{(h^2+x_r^2)^{\frac{(m+2)}{2}}.x_r}$$
$$H_{\text{LED},r}(x) = K(m+1)h^{m+1}(h^2+x_r^2)^{-\frac{(m+2)}{2}}.x_r^{-1} \tag{6}$$

where $K = \frac{1}{2\pi}\gamma^2 n\nu^2$. It is obvious that $H_{\text{LED},r}(x)$ is a monotonically decreasing function with respect to x_r. To find the probability density function (pdf) of channel gain, (6) can be represented in its inverse form as follows:

$$H^{-1}_{\text{LED},r}(H) = \frac{1}{2}[-\lambda \pm (\lambda^2 - 4H^{-\frac{2}{m+2}})^{\frac{1}{2}}] \tag{7}$$

where $\lambda = h^2[K(m+1)h^{m+1}]^{-\frac{2}{m+2}}$. As the inverse function $H^{-1}_{\text{LED},r}$ is differentiable with respect to the change of channel gain, H across $0 < \psi_{\text{LED},r} < \theta_{\text{FOI}}$, we can represent the pdf of $H_{\text{LED},r}$ according to change of variable method

$$\text{PDF}_{H_{\text{LED},r}}(H) = \frac{\partial}{\partial H} \mid H^{-1}_{\text{LED},r}(H) \mid$$
$$= 2(m+2)^{-1}(\lambda^2 - 4H^{-\frac{2}{m+2}})^{-\frac{1}{2}}H^{-\frac{m+4}{m+2}}$$
$$\text{for } H \epsilon [H_{\min}, H_{\max}] \tag{8}$$

where $H_{\min}$ and $H_{\max}$ represent the channel gain at boundary levels, respectively. For OCC system, the signal power at the receiver depends on the transmitted power from LED T_{LED}, optical to electrical conversion efficiency per pixel ξ, the area of projected image in the IS a_{RoI}, the image distortion factor α, and the dc channel gain $H_{\text{LED},r}$ [14]. Hence, the signal-to-interference-noise ratio (SINR) can be represented by (9) considering $(N-1)$ number of interfering LEDs inside the camera

Algorithm 1: Two-Level Power Transmitter for NOMA-OCC.

Input: s_1 ="100110...," s_2 ="010011..."
Output: Superimposed LED state
1: P_1 and P_2 as upper and lower power level;
2: Frequency f_1 and f_2 for "0" & "1," respectively;
3: **for** $i = 0$: length of data sequence **do**
4: **if** clock = "1" **then**
5: take $s_1(i)$ as input;
6: **if** $s_1(i) =$ "0" **then**
7: set LED at P_1 for a time of $1/f_1$;
8: **else**
9: set LED at P_1 for a time of $1/f_2$;
10: **end if**
11: **else**
12: take $s_2(i)$ as input;
13: repeat line 6 to 10 for $s_2(i)$ at P_2;
14: **end if**
15: **end for**

field-of-view and additive white Gaussian noise (AWGN) channel of power η

$$\text{SINR}_{r,\text{LED}} = \frac{(1-\alpha)a_{\text{RoI}}\xi H_{\text{LED},r}T_{\text{LED}}}{\sum_{i=1}^{N-1}(a_{\text{RoI}})_i\xi H_{\text{LED}_i,r}T_{\text{LED}_i}+\eta}. \quad (9)$$

To calculate the achievable bit rate of the users, the captured total bits within the camera frames per second are measured. In the case of our proposed system, even though LED transmits signals for a user at a certain power level, signals are modulated by controlling the LED ON–OFF duration, which are determined from the transmitted payload. The received pixel intensity at the IS depends on the amount of light projected on each pixel. Therefore, longer ON period of an LED generates higher intensity value and shorter ON period generates lower intensity value in the pixels. Furthermore, the received signal quality in the IS is also influenced by other ambient noise sources in the OCC channel. Those noise signals generate signal independent spurious noise current in each pixel. Assuming b_{frame} is the number of bits per frame and R_f is the FR of the camera. Then, the total instant achievable bits per second will be $R_f b_{\text{frame}}$.

Then, according to Shannon–Hartley theorem, channel capacity per user can be represented by the following:

$$C_{\text{user}_i} = R_f b_{\text{frame}} \log_2\left(1+\frac{(1-\alpha)a_{\text{RoI}}\xi H_{\text{LED},r}T_{\text{LED}}}{\sum_{i=1}^{N-1}(a_{\text{RoI}})_i\xi H_{\text{LED}_i,r}T_{\text{LED}_i}+\eta}\right). \quad (10)$$

In order to know the aggregated capacity of all the communication channels in that network, we can represent the sum rate of the system as $R_{\text{sum}} = \sum_{j=1}^{K} C_{\text{user}_j}$ in terms of the angle of irradiance with respect to the LED axis [31].

III. Transmitter Design Based on NOMA-OCC

O-NOMA presented in [27] allows different users to share the same time and frequency resources in power domain, leading to enhance system capacity. Generally, in VLC system, LED transmits data by consecutively high-speed switching between ON and OFF states. In our proposed NOMA-OCC scheme, the same time frame and frequencies are shared to transmit two signals separated in power domain. We used FSOOK to modulate the signals individually and then superimposed together into one signal by controlling the power level. In order to use FSOOK as the technique to modulate LED light according to input bits, two frequencies (mark and space) have to be chosen in such a manner that the mark frequency represents bit "1" and the space frequency represents bit "0". Both channels are modulated using the same frequencies. However, they will not create any interference in the receiver side as the channels are nonorthogonally superimposed by a power difference of the LED. In this article, the proposed NOMA-OCC scheme utilizes two different payloads in order to support multiple access. The bit encoding scheme is illustrated in Fig. 3. In this system, the mark is defined as of lower frequency (2 kHz) and the space is defined as of higher frequency (4 kHz). Consequently, while bit "1" is transmitted through the LED, the camera will capture a longer state and vice versa, as shown in Fig. 3. The input data sequences are encoded according to the clock state, which has to be synchronous with the modulation speed. Sequence s_1 transmits with power P_1 only with the clock at its ON state and sequence s_2 is transmitted with power P_2 with the clock at its OFF state. For example, if s_1 and s_2 have bit sequences "100110" and "010011," respectively, after encoding, the actual input to the LED will be "100100101101" and consequently, each consecutive bit will convey different power levels P_1 and P_2. Therefore, signals are not transmitted into individual time slots. Instead that, both the signals complete the transmission simultaneously within the time frame. Moreover, synchronization between the LED flickering speed and the FR of the receiver is important for avoiding bit loss [32].

The proposed transmitter design procedure is abridged in Algorithm 1. The general hardware components in the transmitter include a fast switching device (metal–oxide–semiconductor module), an Arduino board, a direct current power supply, and an LED [11]. According to the required data transmission, all the modulation and encoding techniques are applied on the payload and programmed using Arduino before being fed into the LED input. According to Algorithm 1, the proposed modulation, encoding, and superimposition of the two different power level signals can be programmed using the LED driver circuit (i.e., Arduino).

In order to validate the proposed encoding scheme of the payload, we developed a real testbed scenario illustrated in Fig. 4. As described in Fig. 1, we considered two smartphone users for inner and outer regions. We programmed the LED driver circuit according to the proposed encoding scheme described in Algorithm 1. In Fig. 4, the captured image of the transmitter is also depicted. As the LED flickers at two power levels, its recorded image contains ON–OFF strips of both power levels. Because of the rolling shutter effect of the camera, the strips of two different intensity levels lay sequentially one after another. These two different types of strips resemble the two signals transmitted using the NOMA-OCC scheme. To extract the signals,

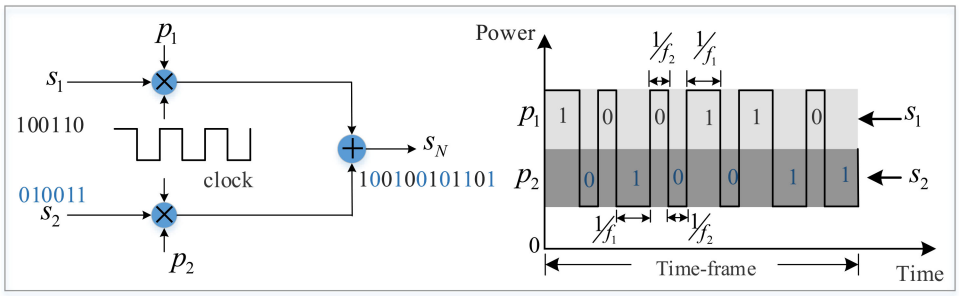

Fig. 3. Data encoding scheme of two-stage power allocation based NOMA-OCC system.

Algorithm 2: Demodulation Scheme at the Receiver.

Input: Captured image of superimposed LED state
Output: $x_1 =$ "100110...," $x_2 =$ "010011..."

```
get image matrix A_{i,j}(r, g, b);
convert to grayscale image A_{i,j}(r, g, b) → G_{i,j}(gray);
threshold to separate strips of power level P_1 and P_2;
get distance D_{r,LED};
if D_{r,LED} > d_max then
    select strips of power P_1 and get strips' widths l(i);
    check channel state information;
    if channel is occupied then
        continue from line 18;
    else
        if l(i) > l_th then
            set x_1(i) = "1";
        else
            set x_1(i) = "0";
        end if
    end if
else
    select strips of power P_2 and get strips' widths l(i);
    check channel state information
    if channel is occupied then
        continue from line 6;
    else
        if l(i) > l_th then
            set x_2(i) = "1";
        else
            set x_2(i) = "0";
        end if
    end if
end if
```

the intensity threshold could be applied and depending on the users' locations, the unnecessary signal could be discarded.

IV. Power Separation in the Receiver

The IS in the smartphone camera or other high-speed cameras consists of a number of unit pixels that capture the light intensity. In the proposed OCC system, as the transmitter is designed to transmit signals through light modulation at the speed of carrier frequency, the camera has the capability of capturing

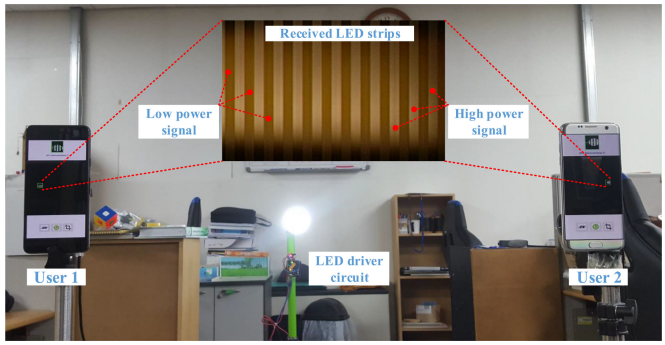

Fig. 4. Experimental setup for analyzing NOMA-OCC transmitter image.

every lighting state by controlling its shutter speed. The camera's rolling shutter mechanism [32] assists in capturing the LED states as horizontal strips. In this system, the LED flickers according to the transmitted bits using two power levels in a 1-b duration. The upper half of a bit contains power P_1, and the lower half of a bit contains power level P_2. When a camera records the LED signal in its consecutive frames, it will capture the strip patterns depending on the power level of the upper portion and lower portion of that signal such that each frame will contain both the signals of different intensities, as shown in Fig. 5. The strips' pattern shown in this figure is vertical due to the rotation of the image view about 270°. This patterns can be separated by applying an intensity threshold value. A smartphone can be a suitable device to implement such an application supporting the region-of-interest (ROI) detection and applying image processing to separate the two received data patterns from each other [11], [20]. Smartphones can support multiple data reception simultaneously from multiple LEDs. However, due to the limitations of the current smartphone camera FR and data rate, one can use high-speed camera (FR up to 1000 ft/s) integrated device to achieve a higher data rate and mobility support. Nevertheless, the necessary image processing libraries, such as openCV must be imported with the software. This library would help to carry out necessary pixel intensity measurement, format changing, pixel grouping, edge selection, and classification by pixel matrix operation [20].

Algorithm 2 describes the data demodulation scheme applied in the receiver side. Currently, common commercial IS are made sensitive to red, green, and blue (RGB) colors to produce

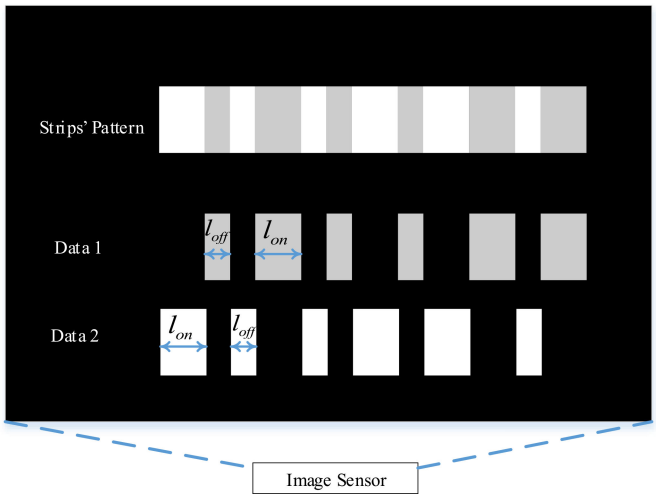

Fig. 5. Two signal separation and data decoding from a captured LED image using intensity threshold in the IS.

color images. This implies that each IS element (known as pixel) conveys three intensity values as pixel information. In the proposed system, only the white LED is of interest. Hence, the RGB values per pixel are not directly used, and only the average value was taken for each pixel. The openCV library supports RGB to grayscale conversion of an image matrix $A_{i,j}(r, g, b)$ by using the command cv2.cvtColor($imagename$, cv2.$COLORBGR2GRAY$) and gives an output of $G_{i,j}$(gray). In the converted image, only the stripped gray-shaded LED region is appeared due to the rolling mechanism of the camera and the dark surrounding region of the LED. The region that consists of the gray-shaded LED is known as LED-ROI. This is the region of bright pixel colonies, where the subsequent operation will be performed.

Because of the superimposed transmission of the two signals of two different power levels P_1 and P_2, the strips in the LED-ROI are of two types, with one group of strip brighter than the other. The next step involves separating the two groups of LED strips of power level P_1 and P_2, as shown in Fig. 5. After that, the measured area of LED-ROI is used to determine the direct distance $D_{r,\text{LED}}$ from the receiver to the LED. If d_{lens} is the distance of the IS from the camera lens and F is the focal length, then we can write from the general lens equation as

$$\frac{d_{\text{lens}}}{D_{r,\text{LED}}} = \frac{F}{D_{r,\text{LED}} - F} = \frac{F}{D_{r,\text{LED}}} \quad \text{for, } F << D. \tag{11}$$

Magnification factor is used to express the relationship between the actual size of the LED and the detected size of that in the IS. Hence, the magnification factor m_{lens} can be represented as

$$m_{\text{lens}} = \sqrt{\frac{a_{\text{RoI}}}{A_{r,\text{LED}}}} = \frac{d_{\text{lens}}}{D_{r,\text{LED}}} \tag{12}$$

$$\text{or } a_{\text{RoI}} = \frac{F^2}{D^2_{r,\text{LED}}} A_{\text{LED}}. \tag{13}$$

Therefore, considering the radial distortion of the shape of LED in the IS, the $D_{r,\text{LED}}$ can be expressed from (13) as

$$D_{r,\text{LED}} = F\sqrt{\frac{\pi l^2 \cos(\delta_{r,\text{LED}})}{a_{\text{RoI}}}} \tag{14}$$

where l is the radius of the circular LED. Users located at a distance greater than $d_{\max}$ ($D_{r,\text{LED}} > d_{\max}$) will experience lower channel gain than the users located close to the vertical LED point ($D_{r,\text{LED}} < d_{\max}$). Hence, if $D_{r,\text{LED}} > d_{\max}$, the user will select the channel of the higher power level P_1. Otherwise, the user can switch to the channel of lower power level P_2. The channel payloads contain the information of channel status, whether it is occupied or not. Thereafter, for the case of first user, it will access the channel based on the region where it is located, and that channel will be occupied for this particular user until it disconnects its LOS connection. In a situation, when the second user enters the same region, it will access the remaining channel irrespective of the region. Otherwise, channel occupancy status will be decoded if it tries to access the same data strips. This similar situation can occur if a third user enters within the LED FOI while two active users are already accessing both the channels. This two-channel separation in the receiver depends on the average pixel intensity difference between the two types of strips pattern. Due to this intensity difference, a threshold value had to be chosen to separate the two groups of LED ON–OFF strips. After acquiring the channel of desired power level, the receiver demodulates the data from the received group of LED strips. This operation must undergo a looping process for every image frame. As the frequency or state duration is different for both digital bits "1" and "0," the width of strips will vary. The higher value of frequency reduces the duration of ON or OFF state and vice versa [16], [20]. In the system developed in this article, the space frequency was considered greater than the mark frequency. These phenomenon indicates that greater width corresponds to bit "1" than bit "0". It is worth mentioning that the covered areas of the strips in the IS varies in the scale of few pixels due to the image distortion. Hence, an pertinent threshold value lth was set to distinguish between the widths correspond to bits "1" and "0", as described in Algorithm 2.

V. Simulation Results

In this section, the performance of the proposed NOMA-OCC framework has been evaluated. A room of size 6 m × 6 m × 2.8 m was considered, which consists of several equally spaced ceiling LEDs. Each LED was set to transmit data according to the proposed method described in Algorithm 1. As a result, each LED allowed two smartphone users to be simultaneously supported using two different allocated channels nonorthogonally. In the case of LED FOI, the receiver experiences other LED signals as interference. However, in those instances, interference would not occur if LED FOIs do not overlap with each other. Considering this phenomenon, to evaluate the SINR values for both users, only the LEDs surrounding the selected LED are considered as interfering LEDs. PDF of an LED channel gain is analyzed to represent the probability distribution of the channel on the light illumination region of the LED. In Fig. 6, the

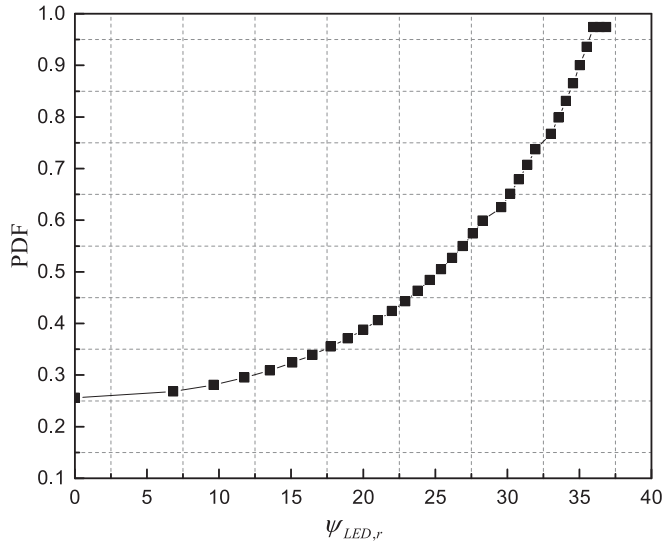

Fig. 6. PDF analysis of channel response within the LEDs' FOI region.

TABLE I
UNCHANGED SYSTEM PARAMETERS

Parameter	Description	Value
h	Vertical height between LED & camera	2.8 m
P_1, P_2	LED power level	15 W, 10 W
f_1, f_2	Mark and space frequency	2 kHZ, 4 kHz
ξ	Optical to electrical conversion efficiency per pixel	1
α	Image distortion factor	0
$\psi_{LED,r}$	Maximum angle of irradiance	37^o
θ_{FOI}	LED FOI	74^o
ν	Pixel dimension of the IS	1.4 μm
γ	Receivers' refractive index	1
d_{max}	Threshold LOS distance	3.15 m
l	LED radius	8.9 cm
m	Lambertian order	1
η	Total noise (AWGN)	$10^{-21}A^2/Hz$
R_f	Camera FR	30, 240, 960 fps
F	Effective focal length	27 mm

pdf of the channel response is illustrated for different angles of irradiance of the LED. Because users can randomly situate within the area of LED coverage while communicating with the LED AP, this angle of irradiance ($\psi_{\text{LED},r}$) is chosen randomly. In this case, the angle $\psi_{\text{LED},r}$ is chosen as a random variable, which has the maximum spread of $0.5\theta_{\text{FOI}}$ (in our simulation, FOI, θ_{FOI} is considered as 74°). LEDs of larger FOIs can provide higher pdf of the channel response. Therefore, the graphical representation of pdf in Fig. 6 shows that it has a maximum value when the angle $\psi_{\text{LED},r}$ reaches its maximum point (37°). The results are calculated within the horizontal coverage up to $2Kh^2(h^2+x_r^2)^{-1.5}x_r^{-1}$ from the vertical LED position, where $m=1$.

A. Channel Capacity Analysis

The two channels are distributed to the users according to the distance between the transmitter and receiver. According to Algorithm 2, channel selection is depended on the channel gain $H_{\text{LED},r}$. The LED FOI is divided virtually into two sections: inner ($H_{\text{LED},r} > (H_{\text{LED},r})_{\text{avg}}$) and outer ($H_{\text{LED},r} < (H_{\text{LED},r})_{\text{avg}}$) region based on the average $H_{\text{LED},r}$. Experimentally, the inner region was found to be within the angle $\psi_{\text{LED},r} = 27.27°$ and the outer region was found to be within the angle $\psi_{\text{LED},r} = 27.27°$–37°. According to the room height and the maximum value of $\psi_{\text{LED},r}$, the diameter of the outer circular region was found to be 4.2 m. All system parameters used for the simulation are summarized in Table I. In this section, the overall channel capacity and the achievable individual data rate are analyzed according to the proposed scheme.

The proposed system says, one LED AP can support two users simultaneously transmitting a pair of signals, which are separated by power domain NOMA scheme. The achievable data rate of each individual user depends on the LOS distance from camera to the LED. Therefore, it is necessary to simulate the sum rate of the LED AP, which is defined as the aggregated capacity

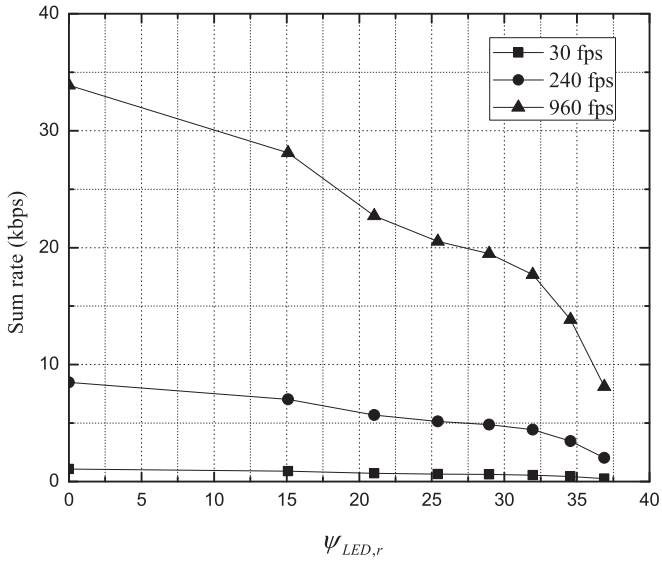

Fig. 7. Sum rate analysis for an LED AP supporting two users within its FOI region.

of all the communication channels in that network. In Fig. 7, the sum rate is expressed according to angle of irradiance with respect to LED axis, where the maximum angle is $0.5\theta_{\text{FOI}}$. The figure also shows the comparison of the sum rates considering three cases of receiver FR: low-speed camera (30 ft/s, e.g., common smartphones), medium-speed camera (240 ft/s, e.g., Google Pixel 4), and high-speed camera (960 ft/s, e.g., Samsung Galaxy S10, Huawei Mate 30 pro). It is worth mentioning that a higher FR camera can provide a higher data rate. Using the proposed scheme, it was found that a sum rate of 34 kb/s can be provided by an LED AP for the receivers set in 960-ft/s camera, whereas it is reduced to 1.2 kb/s in the case of a low FR receiver. Fig. 8(a) and (b) depicts the relationship between the achievable channel capacity with the change of communication distance for both U_1 and U_2, respectively. Even though higher power is

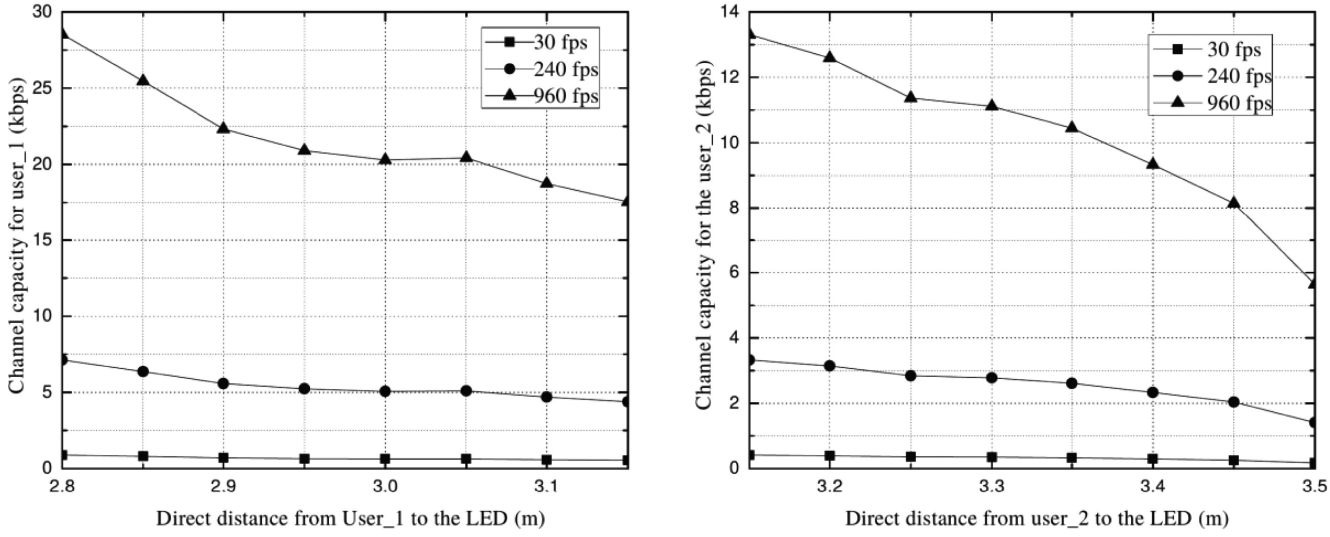

Fig. 8. Channel capacity experienced at different camera FR by the (a) user 1 in the inner region and (b) user 2 in the outer region.

allocated to U_2, U_1 achieved a relatively high data rate because it is located closer to the floor position of the LED. This is due to the number of bits per frame increase with the increase of the LED size in the IS. The simulation results show that the data rate up to 28 kb/s can be achieved by using a camera of 960 ft/s at a communication distance of 2.8 m and it decreases with the increase of communication distance from the LED, as shown in Fig. 8(a) and (b).

B. BER Analysis

The BER in smartphone cameras, based on the OCC system, depends on the channel condition as well as the received image processing mechanism [15]. As U_1 is considered to receive the data of power P_1, it measures the widths of each strip to decode the binary payload of power P_1 and the same procedure is considered for U_2. As mentioned in Algorithm 2, bit "1" signifies the larger width and "0" signifies the shorter width. When the difference between these widths shortens, the probability of decoding an incorrect bit increases. For example, from previous works [11], [20], it was found that the widths of 2–4 pixels and 7–9 pixels are occupied if an LED flickers at the frequency of 4 and 2 kHz, respectively. Therefore, a threshold value (lth ~ 5 or 6 pixels) can be applied to yield error free decoding. In other cases, it can vary according to the exposure of the camera [9]. Bit error probabilities ρ_{u1} and ρ_{u2} for the users U_1 and U_2 can be represented, respectively, as follows:

$$\rho_{u1} = \frac{1}{2} R_f E(l_i) \text{erfc}\left(\sqrt{\frac{Y_{u1}}{(I_{u1}+\eta)}}\right) \tag{15}$$

$$\rho_{u2} = \frac{1}{2} R_f E(l_i) \text{erfc}\left(\sqrt{\frac{Y_{u1}}{(I_{u2}+\eta)}}\right) \tag{16}$$

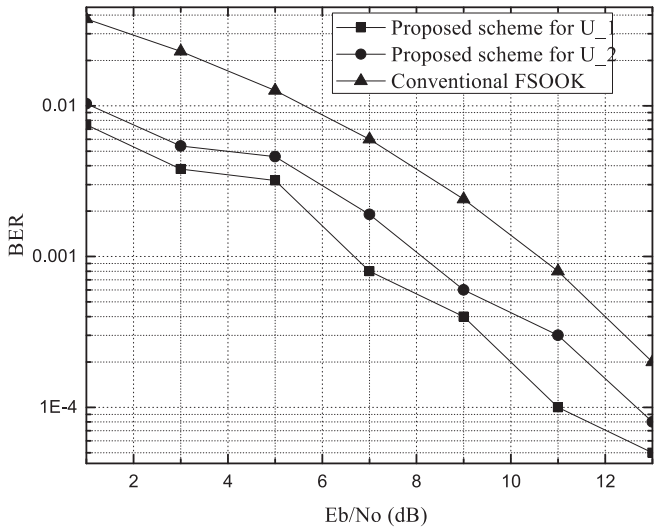

Fig. 9. BER performance of the proposed system.

where the strips error function $E(l_i)$ is introduced to express the probability of occurring bit error per frame due to the measurement of the incorrect strip width. The complementary error function (erfc) is a function of the resultant SINR of the system, where I_u is the interference generated from other LEDs. $E(l_i)$ is expressed as follows:

$$E(l_i) = \begin{cases} \frac{\epsilon_0}{b_{\text{total}}}, & \text{if count 0 for } l_i > l_{\text{th}} \\ \frac{\epsilon_1}{b_{\text{total}}}, & \text{if count 1 for } l_i < l_{\text{th}} \\ \frac{\epsilon_{0,1}}{b_{\text{total}}}, & \text{if count both} \end{cases} \tag{17}$$

where ϵ_0, ϵ_1, and $\epsilon_{0,1}$ are the number of error bits per image frame counted for the respected bits or both and b_{total} is the total number of received bits per frame. Fig. 9 illustrates the BER performance comparison of the proposed NOMA-OCC

enabled FSOOK scheme for both the users U_1 and U_2 with the conventional FSOOK scheme. According to the NOMA-OCC system, we controlled power for the users of both regions. The user in the outer region receives the signal of higher power, whereas the user in the inner region receives signals of lower power. Hence, the power is distributed efficiently to both the users and the number of detected error bits per frame reduces. On the contrary, in conventional FSOOK, only a single user receives signals of same power at every place inside the LED FOI. Therefore, according to the proposed NOMA-OCC scheme, both the users experienced much lower BER (up to the level of 10^{-4}) as opposed to the conventional scheme. The slight variation between the BER performances of U_1 and U_2 is due to the received LED images has reduced size for the edge receiver. Hence, U_1 shows lower BER while the direct communication link distance is closer to the room height.

VI. Conclusion

In this article, a NOMA architecture was proposed to improve the capacity and system performance of the OCC channel. A modulation and encoding scheme based on NOMA for an OCC transmitter were designed, which provides two channels of the same modulation frequency by changing its power domain. Due to the different pixel values displayed by IS according to the incoming light intensity, an intensity-threshold-separation technique in the IS receiver was characterized to distinguish the two channels. To analyze the system performance, simulation results representing the overall sum rate and individual channel capacities were carried out. The simulation results also included a comparison of both channel capacities between the cameras of various FRs (30, 240, and 960 ft/s). It was shown that 28-kb/s data rate was achieved using a smartphone camera set to 960 ft/s at 2.8-m distance. Furthermore, the BER performance of each user channel was evaluated and compared with the conventional FSOOK scheme. The proposed NOMA-OCC exhibited much lower BER performance for the both receivers. On the basis of the overall performance analyses, the proposed scheme can be a promising solution for the improvement of the OCC system performance.

References

[1] A. Al-Kinani, C. Wang, L. Zhou, and W. Zhang, "Optical wireless communication channel measurements and models," *IEEE Commun. Surv. Tut.*, vol. 20, no. 3, pp. 1939–1962, May 2018.

[2] M. Z. Chowdhury, M. T. Hossan, A. Islam, and Y. M. Jang, "A comparative survey of optical wireless technologies: Architectures and applications," *IEEE Access*, vol. 6, pp. 9819–9840, 2018.

[3] P. H. Pathak, X. Feng, P. Hu, and P. Mohapatra, "Visible light communication, networking, and sensing: A survey, potential and challenges," *IEEE Commun. Surv. Tut.*, vol. 17, no. 4, pp. 2047–2077, Sep. 2015.

[4] Z. Ghassemlooy, P. Luo, and S. Zvanovec, "Optical camera communications," in *Optical Wireless Communications,* Cham, Switzerland: Springer, Aug. 2016, pp. 547–568.

[5] H. Chen *et al.*, "Color-shift keying for optical camera communication using a rolling shutter mode," *IEEE Photon. J.*, vol. 11, no. 2, Apr. 2019, Art. no. 7901808.

[6] L. Liu, R. Deng, and L. Chen, "Spatial and time dispersions compensation with double-equalization for optical camera communications," *IEEE Photon. Technol. Lett.*, vol. 31, no. 21, pp. 1753–1756, Oct. 2019.

[7] M. Z. Chowdhury, M. K. Hasan, M. Shahjalal, M. T. Hossan, and Y. M. Jang, "Optical wireless hybrid networks: Trends, opportunities, challenges, and research directions," *IEEE Commun. Surv. Tut.*, vol. 22, no. 2, pp. 930–966, Apr.–Jun. 2020.

[8] N. Chi, "LED-based visible light communications," in *Signals and Communication Technology.* Berlin, Germany: Springer-Verlag, 2018, pp. 1–245.

[9] M. T. Hossan *et al.*, "A new vehicle localization scheme based on combined optical camera communication and photogrammetry," *Mobile Inf. Syst.*, vol. 2018, pp. 1–14, Mar. 2018.

[10] B. Lin, Z. Ghassemlooy, C. Lin, X. Tang, Y. Li, and S. Zhang, "An indoor visible light positioning system based on optical camera communications," *IEEE Photon. Technol. Lett.*, vol. 29, no. 7, pp. 579–582, Apr. 2017.

[11] M. Shahjalal *et al.*, "An implementation approach and performance analysis of image sensor based multilateral indoor localization and navigation system," *Wireless Commun. Mobile Comput.*, vol. 2018, Nov. 2018, Art. no. 7680780.

[12] Y. Li, Z. Ghassemlooy, X. Tang, B. Lin, and Y. Zhang, "A VLC smartphone camera based indoor positioning system," *IEEE Photon. Technol. Lett.*, vol. 30, no. 13, pp. 1171–1174, May 2018.

[13] M. T. Hossan, M. Z. Chowdhury, M. Shahjalal, and Y. M. Jang, "Human bond communication with head-mounted displays: Scope, challenges, solutions, and applications," *IEEE Commun. Mag.*, vol. 57, no. 2, pp. 26–32, Feb. 2019.

[14] T. Yamazato *et al.*, "Vehicle motion and pixel illumination modeling for image sensor based visible light communication," *IEEE J. Sel. Areas Commun.*, vol. 33, no. 9, pp. 1793–1805, Sep. 2015.

[15] A. Căilean and M. Dimian, "Current challenges for visible light communications usage in vehicle applications: A survey," *IEEE Commun. Surv. Tut.*, vol. 19, no. 4, pp. 2681–2703, May 2017.

[16] M. K. Hasan, M. Shahjalal, M. Z. Chowdhury, and Y. M. Jang, "Real-time healthcare data transmission for remote patient monitoring in patch-based hybrid OCC/BLE networks," *Sensors*, vol. 19, no. 5, Mar. 2019, Art. no. 1208.

[17] D. Karunatilaka, F. Zafar, V. Kalavally, and R. Parthiban, "LED based indoor visible light communications: State of the art," *IEEE Commun. Surv. Tut.*, vol. 17, no. 3, pp. 1649–1678, Mar. 2015.

[18] S. Halawi, E. Yaacoub, S. Kassir, and Z. Dawy, "Performance analysis of circular color shift keying in VLC systems with camera-based receivers," *IEEE Trans. Commun.*, vol. 67, no. 6, pp. 4252–4266, Jun. 2019.

[19] L. Chen, W. Wang, and C. Zhang, "Coalition formation for interference management in visible light communication networks," *IEEE Trans. Veh. Technol.*, vol. 66, no. 8, pp. 7278–7285, Aug. 2017.

[20] M. Shahjalal, M. H. Khalid, M. Z. Chowdhury, and Y. M. Jang, "Smartphone camera-based optical wireless communication system: Requirements and implementation challenges," *Electronics*, vol. 8, no. 8, pp. 913–929, Aug. 2019.

[21] H. Marshoud, V. M. Kapinas, G. K. Karagiannidis, and S. Muhaidat, "Non-orthogonal multiple access for visible light communications," *IEEE Photon. Technol. Lett.*, vol. 28, no. 1, pp. 51–54, Jan. 2016.

[22] P. Luo *et al.*, "Experimental demonstration of RGB LED-based optical camera communications," *IEEE Photon. J.*, vol. 7, no. 5, pp. 1–12, Oct. 2015.

[23] P. Luo *et al.*, "Experimental demonstration of a 1024-QAM optical camera communication system," *IEEE Photon. Technol. Lett.*, vol. 28, no. 2, pp. 139–142, Jan. 2016.

[24] Z. Ding, M. Peng, and H. V. Poor, "Cooperative non-orthogonal multiple access in 5G systems," *IEEE Commun. Lett.*, vol. 19, no. 8, pp. 1462–1465, Aug. 2015.

[25] C. Chen, W. Zhong, H. Yang, and P. Du, "On the performance of MIMO-NOMA-based visible light communication systems," *IEEE Photon. Technol. Lett.*, vol. 30, no. 4, pp. 307–310, Feb. 2018.

[26] X. Liu, Y. Wang, F. Zhouz, and R. Q. Hu, 'BER analysis for NOMA-enabled visible light communication systems with M-PSK," in *Proc. 10th Int. Conf. Wireless Commun. Signal Process.*, Hangzhou, China, 2018, pp. 1–7.

[27] H. Marshoud, S. Muhaidat, P. C. Sofotasios, S. Hussain, M. A. Imran, and B. S. Sharif, "Optical non-orthogonal multiple access for visible light communication," *IEEE Wireless Commun.*, vol. 25, no. 2, pp. 82–88, Apr. 2018.

[28] H. Shen, Y. Wu, W. Xu, and C. Zhao, "Optimal power allocation for downlink two-user non-orthogonal multiple access in visible light communication," *J. Commun. Inf. Netw.*, vol. 2, no. 4, pp. 57–64, Dec. 2017.

[29] L. Yin, W. O. Popoola, X. Wu, and H. Haas, "Performance evaluation of non-orthogonal multiple access in visible light communication," *IEEE Trans. Commun.*, vol. 64, no. 12, pp. 5162–5175, Dec. 2016.
[30] S. M. Berman, D. S. Greenhouse, I. L. Bailey, R. D. Clear, and T. W. Raasch, "Human electroretinogram responses to video displays, fluorescent lighting, and other high frequency sources," *Optometry Vis. Sci.*, vol. 68, pp. 645–662, 1991.
[31] H. Shen, Y. Deng, W. Xu, and C. Zhao, "Rate maximization for downlink multiuser visible light communications," *IEEE Access*, vol. 4, pp. 6567–6573, 2016.
[32] H. Y. Lee, H.-M. Lin, Y. Wei, H. Wu, H. Tsai, and K. Lin, "Rollinglight: Enabling line-of-sight light-to-camera communications," in *Proc. 13th Annu. Int. Conf. Mobile Syst.*, Florence, Italy, May 2015, pp. 167–180.

Md. Shahjalal (Student Member, IEEE) received the B.Sc. degree in electrical and electronic engineering from the Khulna University of Engineering & Technology, Khulna, Bangladesh, in 2017, and the M.Sc. degree in electronics engineering in 2019 from Kookmin University, Seoul, South Korea, where he is currently working toward the Ph.D. degree in electronics engineering.

His research interests include optical wireless communications, wireless security, nonorthogonal multiple access, Internet of Things, low-power wide-area network, and 6G mobile communications.

Mr. Shahjalal was the recipient of the Excellent Student Award from Kookmin University.

Moh. Khalid Hasan (Member, IEEE) received the B.Sc. degree in electrical and electronic engineering from the Khulna University of Engineering & Technology, Khulna, Bangladesh, in May 2017, and the M.Sc. degree in electronics engineering, Kookmin University, Seoul, South Korea, in August 2019.

Since September 2019, he has been a full-time Researcher with the Wireless Communication and Artificial Intelligence Laboratory, Department of Electronics Engineering, Kookmin University. His current research interests include wireless communications, 6G, wireless security, and artificial intelligence.

Md. Mainul Islam (Graduate Student Member, IEEE) received the B.Sc. degree in electrical and electronic engineering from the Khulna University of Engineering & Technology, Khulna, Bangladesh, in 2018. He is currently working toward the M.Sc. degree in electronics engineering with the Wireless Communication and Artificial Intelligence Laboratory, Kookmin University, Seoul, South Korea.

His research interests include wireless communication security, blockchain, cryptography, elliptic curve cryptography, Edwards-curve digital signature algorithm, IoT security, VLSI design, 5G, and 6G.

Mr. Islam served as a Reviewer for the IEEE SYSTEMS JOURNAL and *Transactions on Emerging Telecommunications Technologies*.

Mostafa Zaman Chowdhury (Senior Member, IEEE) received the B.Sc. degree in electrical and electronic engineering from the Khulna University of Engineering and Technology (KUET), Khulna, Bangladesh, in 2002, and the M.Sc. and Ph.D. degrees in electronics engineering from Kookmin University, Seoul, South Korea, in 2008 and 2012, respectively.

In 2003, he joined the Department of Electrical and Electronic Engineering, KUET, as a Lecturer, where he is currently a Professor. He was a Postdoctoral Researcher with Kookmin University from 2017 to 2019. He has authored or coauthored around 130 research papers in national and international conferences and journals. His research interests include convergence networks, QoS provisioning, small-cell networks, Internet of Things, eHealth, 5G and beyond communications, and optical wireless communication.

Prof. Chowdhury was the recipient of the Excellent Student Award from Kookmin University in 2008. His three papers received the Best Paper Award at several international conferences around the world. He was involved in many Korean government projects. He was also the recipient of the Best Reviewer Award 2018 by *ICT Express journal*, and the Education and Research Award 2018 given by Bangladesh Community in South Korea. He was a TPC Chair of the International Workshop on 5G/6G Mobile Communications in 2017 and 2018. He was the Publicity Chair of the International Conference on Artificial Intelligence in Information and Communication, in 2019 and 2020. He served as a Reviewer for many international journals (including IEEE, Elsevier, Springer, ScienceDirect, and Hindawi published journals) and IEEE conferences. He is an Editor for *ICT Express*, an Associate Editor for the IEEE ACCESS, a Lead Guest Editor for the *Wireless Communications and Mobile Computing*, and a Guest Editor for the *Applied Sciences*. He has served as a TPC Member for several IEEE conferences.

Yeong Min Jang (Member, IEEE) received the B.E. and M.E. degrees in electronics engineering from Kyungpook National University, Daegu, South Korea, in 1985 and 1987, respectively, and the Doctoral degree in computer science from the University of Massachusetts, Amherst, MA, USA, in 1999.

He was with the Electronics and Telecommunications Research Institute from 1987 to 2000. Since 2002, he has been with the School of Electrical Engineering, Kookmin University, Seoul, South Korea, where he was the Director of the Ubiquitous IT Convergence Center in 2005 and 2010, and has been the Director of the LED Convergence Research Center since 2010 and the Director of the Internet of Energy Research Center since 2018. He is currently a Life Member of the Korean Institute of Communications and Information Sciences. His research interests include 5G/6G mobile communications, Internet of energy, IoT platform, AI platform, eHealth, smart factory, optical wireless communications, optical camera communication, and the Internet of Things.

Prof. Jang has organized several conferences and workshops, such as the International Conference on Ubiquitous and Future Networks from 2009 to 2017, the International Conference on ICT Convergence from 2010 to 2016, the International Conference on AI in Information and Communication from 2019 to 2021, the International Conference on Information Networking in 2015, and the International Workshop on Optical Wireless LED Communication Networks from 2013 to 2016. He was the recipient of the Young Science Award from the Korean Government from 2003 to 2006. He had served as the Founding Chair of the KICS Technical Committee on Communication Networks in 2007 and 2008. He was the Executive Director of KICS from 2006 to 2014, the Vice President of KICS from 2014 to 2016, and an Executive Vice President of KICS in 2018. He was the President of KICS in 2019. He serves as the Co-Editor-in-Chief for the *ICT Express* (Elsevier). He was the Steering Chair of the Multi-Screen Service Forum from 2011 to 2019 and has been the Steering Chair of the Society Safety System Forum since 2015. He served as the Chairman of the IEEE 802.15 Optical Camera Communications Study Group in 2014 and the IEEE 802.15.7m Optical Wireless Communications TG. He successfully published IEEE 802.15.7–2018 standard. He is currently the Chairman of IEEE 802.15 VAT IG.